Collision-energy-resolved Penning ionization electron spectroscopy of bromomethanes (CH3Br, CH2Br2, and CHBr3) by collision with He*(23S) metastable atoms

doi: 10.1063/1.1769367

Collision-energy-resolved Penning ionization electron spectroscopy of bromomethanes (CH_3Br, CH_2Br_2, and $CHBr_3$) by collision with He*($2\,^3S$) metastable atoms

Naoki Kishimoto, Eiichi Matsumura, and Koichi Ohno
Department of Chemistry, Graduate School of Science, Tohoku University, Aoba-ku, Sendai 980-8578, Japan

Michael S. Deleuze
Limburgs Universitair Centrum, Department SBG, Universitaire Campus, B-3590 Diepenbeek, Belgium

(Received 5 April 2004; accepted 17 May 2004)

Ionization of bromomethanes (CH_3Br, CH_2Br_2, and $CHBr_3$) upon collision with metastable He*($2\,^3S$) atoms has been studied by means of collision-energy-resolved Penning ionization electron spectroscopy. Lone-pair (n_{Br}) orbitals of Br_{4p} characters have larger ionization cross sections than $\sigma_{C\text{-}Br}$ orbitals. The collision-energy dependence of the partial ionization cross sections shows that the interaction potential between the molecule and the He*($2\,^3S$) atom is highly anisotropic around CH_3Br or CH_2Br_2, while isotropic attractive interactions are found for $CHBr_3$. Bands observed at electron energies of ~2 eV in the He*($2\,^3S$) Penning ionization electron spectra (PIES) of CH_2Br_2 and $CHBr_3$ have no counterpart in ultraviolet (He I) photoionization spectra and theoretical (third-order algebraic diagrammatic construction) one-electron and shake-up ionization spectra. Energy analysis of the processes involved demonstrates that these bands and further bands overlapping with $\sigma_{C\text{-}Br}$ or π_{CH_2} levels are related to autoionization of dissociating (He^+-Br^-) pairs. Similarly, a band at an electron energy of ~1 eV in the He*($2\,^3S$) PIES spectra of CH_3Br has been ascribed to autoionizing Br** atoms released by dissociation of (unidentified) excited states of the target molecule. A further autoionization (S) band can be discerned at ~1 eV below the lone-pair n_{Br} bands in the He*($2\,^3S$) PIES spectrum of $CHBr_3$. This band has been ascribed to the decay of autoionizing Rydberg states of the target molecule (M**) into vibrationally excited states of the molecular ion. It was found that for this transition, the interaction potential that prevails in the entrance channel is merely attractive. © *2004 American Institute of Physics.*
[DOI: 10.1063/1.1769367]

I. INTRODUCTION

Photoelectron spectroscopies are routinely used nowadays for studying in detail the electronic structure of molecules, polymers, or solids. Spectra measured in vacuum by means of photoelectron techniques provide straightforward access[1–3] to transition energies between the ground state of the molecular target (M) and electronic states of the corresponding molecular cation (M_i^+). In a depiction that does not cope with configuration interactions in the cation and, thus, shake-up transitions, the measured ionization energies are simply equal to one-electron binding energies. Upon neglecting completely the effects of electron correlation and relaxation, these, in turn, relate to orbital energies, according to Koopmans' theorem and Hartree-Fock theory.[2]

Besides providing information on ionization energies, Penning ionization electron spectroscopy[4,5] is also known as one of the most suited methods for probing the shape and spread of molecular orbitals. The transitions studied by this spectroscopy are the result of collisional chemiionization processes between a molecular target (M) and rare gas atoms in metastable excited states. In the electron exchange mechanism proposed for Penning ionization ($A^*+M\rightarrow A+M_i^+ +e^-$),[6,7] an electron in a molecular orbital φ_i of the molecular target M is transferred to the lowest unoccupied orbital of A^*, whereas the excited electron in A^* is ejected, provided A^* has a larger excitation energy than the energy required for ionizing an electron in orbital φ_i. In a molecular orbital (MO) picture (or quasiparticle picture) of ionization, the excess kinetic energy of the ejected electron is thus simply the difference between the excitation energy of the rare gas atom and the electron-binding energy of an electron in orbital φ_i. In a hard-sphere depiction, the probability of the electron transfer and, thus, the related cross section mainly depend on the overlap during the collision between the lowest unoccupied orbital of A^* and the ionized molecular orbital φ_i of M, outside the collision boundary surface.

On the basis of the electron-exchange mechanism, branching ratios of Penning ionization probabilities can be reliably studied by means of the exterior electron density (EED) model.[8–10] In this model, EED are defined for individual MOs,

$$(\mathrm{EED})_i=\int_\Omega |\varphi_i(r)|^2 dr, \tag{1}$$

where Ω is the subspace outside the repulsive molecular surface. EED values calculated with *ab initio* MOs and using as repulsive molecular surface the envelope defined by rigid van der Waals spheres are known[9,10] to provide consistent

insights into the relative intensities of bands in Penning ionization electron spectra (PIES).[9,10] The interaction potential energy surface between A^* and M can, however, be highly anisotropic, and branching ratios (partial ionization cross sections) can strongly vary as a function of the collision energy.[11,12]

According to a two-potential curve model,[13] the kinetic energy of the ejected electron (in short, the electron energy) in a Penning ionization process is equal to the energy difference between the incoming potential curve for the entrance channel (A^*+M) and the outgoing potential curve for the exit channel $(A+M_i^+)$. Therefore, assuming a flat potential curve for the exit channel, the shifts in the electron energies (ΔE) characterizing the position of peaks in PIES relative to the ionization potentials (IPs) measured from ultraviolet photoelectron spectra (UPS) can in principle be used to extract information on the anisotropy of the interaction potential between the atomic probe A^* and the molecular target M. However, in many cases, the potential energy curves for the exit channels may not be flat, and much more sophisticated approaches have to be considered for obtaining experimentally reliable information on the stereodynamics of the reaction embodied in a Penning ionization process and on the anisotropy of the interactions involved in such a process.

One of these approaches is the so-called collision-energy/electron-energy-resolved two-dimensional Penning ionization electron spectroscopy (2D-PIES).[14] In contrast with measurements of the collision-energy dependence of *total* ionization cross sections through a count of ion signals,[15–18] ionic-state-selected measurements of the collision-energy dependence of *partial* ionization cross sections[11,12] (CEDPICS) enable straightforward studies of the anisotropy, outside the collision boundary surface of M, of the interaction potential energy surface between the atomic probe A^* and the molecular target M for each ionization channel (i.e., for each ionized orbital φ_i, in an orbital picture of ionization).

Attractive interactions have been found previously around halogen atoms of $(CH_3)_3CCl$,[19] $C_2H_2Cl_2$,[20] $CH_2{=}{=}CHX$ $(X=Cl,I)$,[21] C_2H_5X $(X=F,Cl)$,[22] and C_6H_5X $(X=F,Cl,Br,I)$,[23] while the σ_{CH} orbital region appears to be repulsive upon collision with $He^*(2\,^3S)$ atomic probes. On the other hand, the interaction around the halogen atom X is highly anisotropic. When $X=F$, the interaction potential along an axis perpendicular to the C-F bond is less attractive than for a collinear direction approach.[22,23] The opposite was found when $X=Cl$, Br, and I; specifically, in these cases, the potential along an axis perpendicular to the C-X axis is more attractive than for a collinear direction approach.[21–23]

Besides the bands relating to an electron exchange Penning ionization process, bands due to autoionization via superexcited species[24–33] are occasionally seen in PIES experiments. These bands are nowadays raising considerable interest. For instance, autoionization bands of superexcited Cl, Br, or S species (S*) produced by dissociation processes have been identified in 2D-PIES studies of HCl,[29] CH_2ClI,[30] CH_2BrCl,[32] $CHBrCl_2$,[32] CS_2,[31] and OCS.[33] The collision-energy dependence of the ionization cross sections of these autoionization bands in the PIES of HCl,[29] CH_2ClI,[30] CH_2BrCl, and $CHBrCl_2$ (Ref. 32) exhibits a reduced (negative) collision-energy dependence compared with that found for the cross sections of the outermost nonbonding MO levels. For instance, the slope parameter m of the linear regression of the cross sections as a function of the collision energy amounts typically to $m=-0.15$ when the band relates to autoionization of superexcited Br atom,[32] whereas $m=-0.35$ for the electron exchange ionization bands associated with n_{Br} lone pairs.[32]

Another type of bands (referred to as S bands), which are thought to be induced by excitation transfer $[A^*+M \rightarrow (A-M)^{**}]$ and autoionization of Rydberg states into vibrationally excited states of the molecular ion, was observed near the n_X lone-pair (n_X) bands of HCl,[27(a),29] HI,[27(c)] and CH_2ClI.[30] These bands exhibit CEDPICS characterized by strongly negative slopes, for instance, $m=-0.38$ and $m=-0.37$ with HCl and CH_2ClI, respectively, and usually take the form of a shoulder with very limited intensity on the lower electron energy side of the n_X bands produced by electron exchange Penning ionization processes.

In continuation to these studies, the main purpose of the present work was to investigate the stereodynamics of Penning ionization of bromomethanes (CH_3Br, CH_2Br_2, and $CHBr_3$) and the anisotropy of the interaction potentials in these processes by means of 2D-PIES measurements, in conjunction with model potential calculations, and EED studies of model Penning ionization cross sections. In the course of the study, autoionization bands of the S and S* types have been identified by comparison with available He I UPS, and benchmark one-particle Green's function (1p-GF) calculations of one-electron and shake-up ionization spectra. These extra autoionization bands have also been systematically studied by means of 2D-PIES, in order to unravel the main features of the related ionization mechanism.

II. EXPERIMENT

The experimental apparatus for $He^*(2\,^3S)$ PIES and He I UPS has been reported previously.[12,14,19] In our experimental setup, beams of metastable and electronically excited helium atoms were produced by a discharge nozzle source with a tantalum hollow cathode. The $He^*(2\,^1S)$ component was quenched by a water-cooled helium discharge lamp. He I UPS were measured by using the He I resonance photons (584 Å, 21.22 eV) produced by a discharge in pure helium gas. The background pressure in a reaction chamber was of the order of 10^{-7} Torr. Sample molecules were purified under vacuum condition. The kinetic energy of ejected electrons was measured by a hemispherical electrostatic deflection type analyzer using an electron collection angle of 90° relative to the incident $He^*(2\,^3S)$ or photon beam. Measurement of the full width at half maximum (FWHM) of the $Ar^+(^2P_{3/2})$ peak in the He I UPS led to an estimate of 60 meV for the energy resolution of the electron energy analyzer. The transmission efficiency curve of the electron energy analyzer was determined by comparing our UPS data of some molecules with those by Gardner and Samson[34] and Kimura *et al.*[35] Calibration of the electron energy scale was

made by reference to the lowest ionic state of N_2 mixed with the sample molecule in He I UPS ($E_c = 5.639$ eV, Ref. 36) and He*($2\,^3S$) PIES ($E_e = 4.292$ eV, Ref. 37), taking into account a peak energy shift of 50 meV in PIES due to repulsive interaction between He* and N_2, and the difference between the lowest IP and the metastable excitation energy [He*($2\,^3S$) = 19.82 eV].

In the experimental setup for the collision-energy-resolved Penning ionization measurement, the metastable atom beam was modulated by a pseudorandom chopper,[38] and then introduced into a reaction cell located at 504 mm downstream from the chopper disk. The measured Penning ionization spectra $I_e(E_e,t)$ were stored as a function of the electron kinetic energy E_e and time t. The resolution of the analyzer was lowered to 250 meV in order to obtain higher counting rates of Penning electrons. Analysis of the time-dependent Penning ionization spectra $I_e(E_e,t)$ by means of the Hadamard transformation,[38] normalized by the velocity distribution of the He* beam, can lead to a two-dimensional mapping of the Penning ionization cross section as functions $[\sigma(E_e,E_c)]$ of the electron energies E_e and collision energies E_c. The velocity distribution in the metastable atom beam was determined by monitoring secondary electrons emitted from a stainless steel plate inserted in the reaction cell.

III. CALCULATIONS

We performed Hartree-Fock (HF) self-consistent field (SCF) calculations in order to obtain electron density maps. The geometries of the neutral target molecules were selected from experimental studies.[39–41] In the electron density contour maps shown in the sequel, thick solid curves indicate the repulsive molecular surface approximated by atomic spheres of van der Waals radii,[42] which have been used to calculate EED values to each MO of the SCF model. The HF-SCF and EED calculations were performed using the 6-31+G* basis set.

Vertical ionization spectra have been computed within the framework of 1p-GF theory and the so-called third-order algebraic diagrammatic construction [ADC(3)] scheme,[43] by means of the original code interfaced to the GAMESS package of programs[44] and using Dunning's aug-cc-pVDZ basis set.[45] With the 1p-GF/ADC(3) approach, the primary one-hole and shake-up two-hole-one-particle ionization energies are recovered through third and first order in correlation, respectively. Constant self-energy diagrams have been computed through fourth order in correlation, using charge-consistent[46] one-electron densities. A threshold on pole strengths of 0.005 has been retained for solving the ADC(3) secular equation, using a Block-Davidson diagonalization procedure[47] in the final diagonalization step [see Ref. 43(d)]. The assumption of frozen core electrons has been used throughout, and symmetry has been exploited to the extent of the largest abelian subgroup of the full molecular symmetry point group. The ADC(3) ionization spectra are also compared with the results of simpler outer-valence Green's function[48] (OVGF) calculations performed with the GAUSSIAN98 package of programs.[49] All OVGF and ADC(3) calculations discussed in the present study are based on molecular geometries that have been optimized using the aug-cc-pVDZ basis set, density functional theory (DFT) in conjunction with the nonlocal hybrid, and gradient corrected Becke three-parameter Lee-Yang-Parr functional[50] (B3LYP) [an approach which is known to provide structural results of quality comparable to that achieved at the benchmark CCSD(T) theoretical level[51]].

Interaction potential curves V^* between He*($2\,^3S$) and the targets for various directions were also calculated on the basis of the well-known resemblance[7] between the He*($2\,^3S$) and Li($2\,^2S$) species in collision processes. More specifically the velocity dependence of the total scattering cross section of He*($2\,^3S$) by He, Ar, and Kr very closely matches that of Li.[52] Furthermore, the He*($2\,^3S$) and Li($2\,^2S$) probes have very similar interaction potential with various targets,[53,54] both for the location and the depth of the well. In a recent study of atomic targets (H, Li, Na, K, and Hg),[55] it has been shown that the interaction potential with He*($2\,^3S$) probes is very faithfully reproduced, within ratios from 1.1 to 1.2 on the depth of the well, by the Li model potential. With regards to these findings and the difficulties arising with calculations of potential energy surfaces for excited states, the Li($2\,^2S$) atom was used in place of the He*($2\,^3S$) atom. Thus, the interaction potential between the

TABLE I. Assignment of the Penning ionization spectrum of CH_3Br, by comparison with ultraviolet photoemission and theoretical [OVGF and ADC(3)] spectra, EED values, or CEDPICS slope parameters m. Ionization potentials and the peak energy shift ΔE in PIES are in eV and meV, respectively. OVGF and ADC(3) pole strengths are given in bracket.

Band	IP_{UPS}	IP_{OVGF}	$IP_{ADC(3)}$[c,d]	MO	EED	ΔE	m
CH_3Br							
1	10.44	10.60 (0.92)	10.52 (0.92)	$6e\ (n_{Br},e_{3/2})$	10.42	−150	−0.34
2[a]	10.77	⋯	⋯	$6e\ (n_{Br},e_{1/2})$		−150	−0.35
3	13.21	13.40 (0.92)	13.41 (0.91)	$10a_1\ (\sigma_{C\text{-}Br})$	2.76	−130	−0.20
4, 5	15.01	15.37 (0.90)	15.51 (0.89)	$5e\ (\pi_{CH})$	6.66	(+30)	−0.05
S*	(18.8)[b]	⋯	⋯	⋯	⋯	⋯	−0.10

[a]Observed by spin-orbit interaction.
[b]Estimated by He*($2\,^3S$) PIES.
[c]Ionization lines for the $9a_1$ orbital have been identified at binding energies of 21.13 (pole strength=0.48), 22.74 (0.13), and 23.33 eV (0.10).
[d]Ionization lines for the $8a_1$ orbital have been identified at binding energies of 24.45 (pole strength=0.22), 24.96 (0.15), and 25.37 eV (0.15).

TABLE II. Assignment of the Penning ionization spectrum of CH_2Br_2, by comparison with ultraviolet photoemission and theoretical [OVGF and ADC(3)] spectra, EED values, or CEDPICS slope parameters *m*. Ionization potentials and the peak energy shift ΔE in PIES are in eV and meV, respectively. OVGF and ADC(3) pole strengths are given in bracket.

Band	IP_{UPS}	IP_{OVGF}	$IP_{ADC(3)}$[b,c]	MO	EED	ΔE	*m*
CH_2Br_2							
1	10.52	10.60 (0.92)	10.52 (0.91)	$13b_2$ ($n_{Br\parallel}$)	3.10	−130	−0.35
2	10.74	10.77 (0.92)	10.70 (0.91)	$6b_1$ ($n_{Br\perp}$)	3.45	−120	
3	11.21	11.14 (0.91)	11.04 (0.90)	$5a_2$ ($n_{Br\perp}$)	3.52	−130	−0.36
4	(11.3)	11.20 (0.92)	11.13 (0.90)	$15a_1$ ($n_{Br\parallel}$)	3.56	⋯	
5	14.05	14.02 (0.91)	14.06 (0.89)	$12b_2$ ($\sigma_{C\text{-}Br}$)	1.94	−70	−0.26
6	14.68	14.67 (0.90)	14.71 (0.86)	$14a_1$ ($\sigma_{C\text{-}Br}$)	2.52	−140	−0.28
7	16.34	16.30 (0.89)	16.38 (0.24), 16.63 (0.62)	$5b_1$ (π_{CH_2})	2.74	⋯	−0.22
S*	(17.7)[a]	⋯	⋯	⋯	⋯	⋯	−0.30
8	19.3	21.30 (0.81)	20.97 (0.53), 22.52 (0.07)	$13a_1$ (C_{2s})	⋯	⋯	⋯

[a]Estimated by He*($2\,^3S$) PIES.
[b]Ionization lines for the $11b_2$ orbital have been identified at binding energies of 22.30 (pole strength=0.06), 22.52 (0.07), and 23.86 eV (0.22).
[c]Ionization lines for the $12a_1$ MO orbital have been identified at binding energies of 25.83 (pole strength=0.07), 25.90 (0.08), and 26.11 eV (0.09).

molecular target and an incoming He*($2\,^3S$) atom has been calculated along various direction approaches using a model Li($2\,^2S$) probe, at the level of second-order Møller-Plesset perturbation theory (MP2), in conjunction with a 6-31+G* basis set.

IV. RESULTS

In Tables I–III, we compare the ionization potentials obtained from UPS measurements on CH_3Br, CH_2Br_2, and $CHBr_3$, with the results of the OVGF and ADC(3) calculations on these compounds. In these tables, all theoretical IPs characterized by a pole strength larger than 0.05 have been listed. We also provide the peak energy shifts in PIES (ΔE) with respect to the nominal energy E_0 (defined as the difference between the metastable excitation energy of the He* probe and the UPS value for the target (IP) together with the calculated EED values and the slope parameters characterizing the measured CEDPICS (*m*). These slope parameters were obtained by a least-squares method for collision energies ranging from 100 to 300 meV.

The experimental UPS (He I) and He*($2\,^3S$) PIES of CH_3Br, CH_2Br_2, and $CHBr_3$ are displayed in Figs. 1–3, respectively, and compared with theoretical ADC(3)/aug-cc-pVDZ spike spectra. In the latter spectra, line intensities are simply scaled according to the computed pole strengths. The electron energy scale of the He*($2\,^3S$) PIES measurements was shifted by 1.40 eV relative to the He I UPS records, according to the difference in the respective excitation energies (21.22–19.82 eV). In these figures, the calculated EED values are also displayed in the form of simulated spectra, using the band positions and band widths that were measured in the He I spectra. For the bands splitted by spin-orbit interactions (e.g., bands 1, 2 of CH_3Br as well as bands 2, 3 and 5, 6 of $CHBr_3$), the energy splitting was estimated from UPS, and the EED value for the individual lines was divided equivalently in the simulated EED spectrum. Striking features in the PIES of CH_3Br (Fig. 1), CH_2Br_2 (Fig. 2), and $CHBr_3$ (Fig. 3) are the bands labeled S*, at electron energies around ~1 or ~2 eV. These bands are missing in the He I

TABLE III. Assignment of the Penning ionization spectrum of $CHBr_3$, by comparison with ultraviolet photoemission and theoretical [OVGF and ADC(3)] spectra, EED values or CEDPICS slope parameters *m*. Ionization potentials and the peak energy shift ΔE in PIES are in eV and meV, respectively. OVGF and ADC(3) pole strengths are given in bracket.

Band	IP_{UPS}	IP_{OVGF}	$IP_{ADC(3)}$	MO	EED	ΔE	*m*
$CHBr_3$							
1	10.40	10.46 (0.91)	10.38 (0.90)	$5a_2$ ($n_{Br\parallel}$)	3.61	−110	−0.48
2	10.74	10.99 (0.92)	10.98 (0.90)	$15a_1$ ($n_{Br\perp}$)	5.16	−130	−0.47
3, 4[a]	10.83	10.89 (0.91)	10.84 (0.90)	$18e$ ($n_{Br\perp}$)	9.30	⋯	−0.45
5, 6[b]	11.64	11.65 (0.91)	11.59 (0.89)	$17e$ ($n_{Br\parallel}$)	9.70	−130	−0.47
S	(12.7)[c]	⋯	⋯	⋯	⋯	⋯	−0.48
7, 8	14.65	14.62 (0.90)	14.72 (0.85)	$16e$ ($\sigma_{C\text{-}Br}$)	4.22	(−170)	−0.48
9	15.85	15.83 (0.89)	15.82 (0.19), 16.01 (0.39), 16.32 (0.22)	$14a_1$ ($\sigma_{C\text{-}Br:CH}$)	2.35	(−50)	−0.45
S*	(17.9)[c]	⋯	⋯	⋯	⋯	⋯	−0.48
10	(19.3)	20.66 (0.82)	20.18 (0.08), 20.29 (0.06), 20.36 (0.06) 20.56 (0.14), 20.80 (0.22), 21.10 (0.06)	$13a_1$ (C_{2s})	⋯	⋯	⋯

[a]Observed by spin-orbit interaction with splitting energy of 0.38 eV.
[b]Observed by spin-orbit interaction with splitting energy of 0.14 eV.
[c]Estimated by He*($2\,^3S$) PIES.

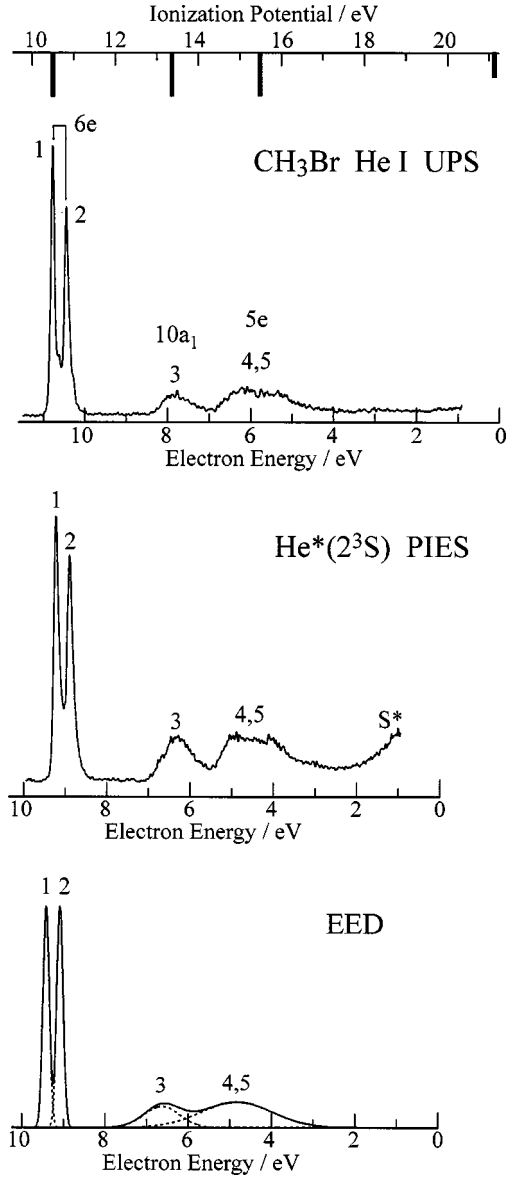

FIG. 1. Comparison of the He I UPS and He*($2\,^3S$) PIES of CH_3Br with the theoretical ADC(3) spike spectrum (above) and an EED simulation (below).

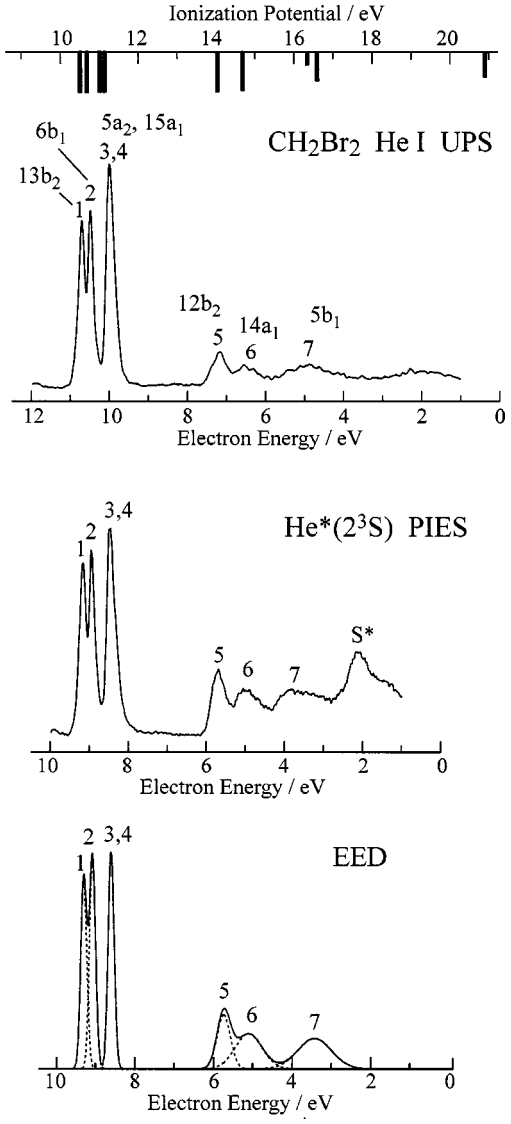

FIG. 2. Comparison of the He I UPS and He*($2\,^3S$) PIES of CH_2Br_2 compared with the theoretical ADC(3) spike spectrum (above) and an EED simulation (below).

UPS records and cannot be accounted for by the ADC(3) calculations.

He*($2\,^3S$) CERPIES (collision-energy-resolved PIES) of CH_3Br and CH_2Br_2 are shown in Figs. 4 and 5, respectively, for collision energies of ~100 (dashed curve) and ~200 meV (solid curve). In Fig. 6, we compare the He*($2\,^3S$) and Ne*($3\,^3P_{0,2}$) CERPIES of $CHBr_3$, taken also at collision energies of ~100 (dashed curve) and ~200 meV (solid curve). In the latter figure, the electron energy scale of the Ne*($3\,^3P_{0,2}$) CERPIES measurements has been shifted relative to that of the He*($2\,^3S$) CERPIES according to a difference of 3.10 eV (=19.82−16.72) between the He*($2\,^3S$) and Ne*($3\,^3P_0$) excitation energies. In that figure, solid arrows give the energy location in the PIES spectrum of the electrons released by an autoionizing dissociation of the molecule into $CHBr_2$. in its ground state and the three lowest electronic configurations of the Br^+ radical cation (see Sec. VI). A further autoionization band S, which will also be discussed in the sequel, is seen below the outermost lone pairs (n_{Br}) in the PIES of $CHBr_3$ (Figs. 3 and 6).

The collision-energy dependences of the partial ionization cross sections (CEDPICS) of CH_3Br, CH_2Br_2, and $CHBr_3$ are displayed as $\ln E_c$ vs. $\ln \sigma$ plots in Figs. 7–9, respectively. These CEDPICS plots were obtained from the 2D-PIES measurements within an appropriate range of electron energies, typically in electron energy intervals equal to the resolution of the spectrometer, i.e., ~250 meV, to avoid a contamination from neighboring bands. Molecular orbital density contour maps are also shown in the figures, along with the employed cutting planes.

Figure 10 shows interaction potential energy curves $V^*(R)$ as functions of the distance R between the model Li probe and (a) CH_3Br, (b) CH_2Br_2, and (c) $CHBr_3$ along various direction approaches.

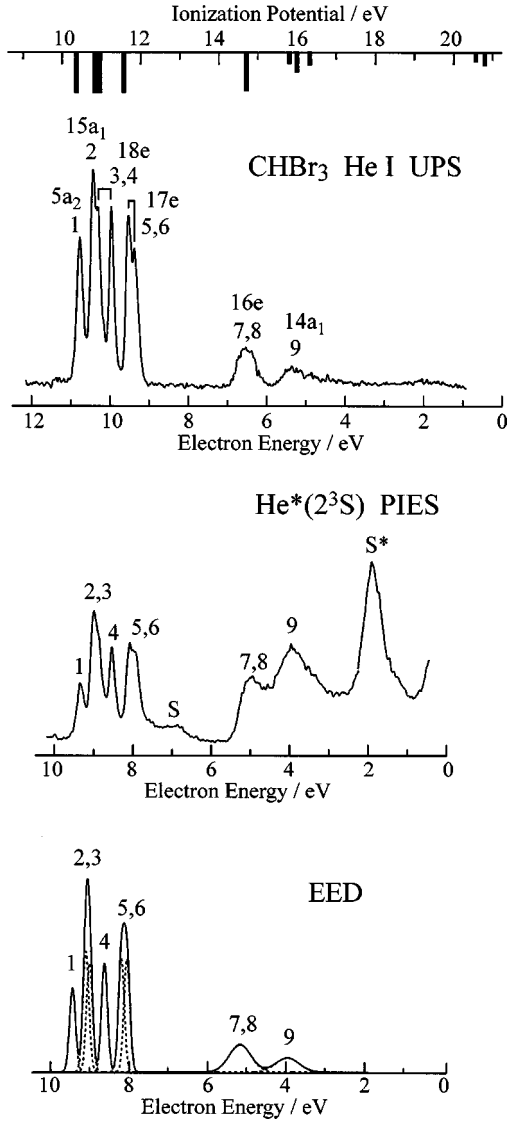

FIG. 3. Comparison of the He I UPS and He*($2\,^3S$) PIES of $CHBr_3$ compared with the theoretical ADC(3) spike spectrum (above) and an EED simulation (below).

V. DISCUSSION OF THE ANISOTROPIES OF INTERACTIONS AROUND CH_3Br, CH_2Br_2, AND $CHBr_3$

The electronic structure of bromomethanes has already been amply studied by means of ultraviolet photoemission spectroscopy.[1,2,35,56–61] It is well known that the nonbonding orbitals of methyl halides are affected by SO interactions.[2] For these electron levels, band splitting is further complicated by vibronic interactions and Jahn-Teller effects.[2,57,58] The ionization energies of the n_{Br} bands in these compounds have been calculated previously on rather questionable semiempirical grounds.[59] He* PIES[61] data and a photoelectron spectrum by synchrotron radiation[62] are also available for CH_3Br.

A. CH_3Br

The first two (1,2) bands in the Penning ionization electron spectrum of CH_3Br are due to ionization of the outermost lone-pair orbitals (n_{Br}, $^2E_{3/2,1/2}$), of dominantly Br_{4p} character. These bands emerge with strong intensity in the

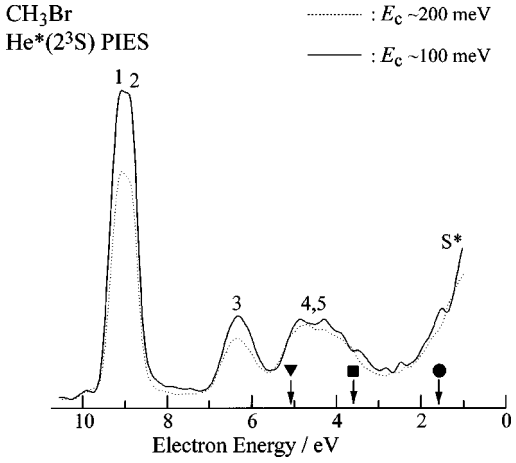

FIG. 4. Collision-energy-resolved He*($2\,^3S$) PIES of CH_3Br (solid curve at 100 meV and dashed curve at 200 meV). Arrows indicate estimates of the energy of electrons released through autoionization of a Br* atom into the $^3P_2$ (▼), $^1D_2$ (■), and $^1S_0$ (●) states of the Br^+ ion (see text).

PIES of Fig. 1 and exhibit a strong collision energy dependence in CEDPICS or CERPIES experiments (Figs. 4 and 7, respectively). The large PIES intensities of bands 1 and 2 can be related to the large EED value found for the doubly degenerate $6e$ orbital. As in UPS, it is found that band 1 has larger intensity than band 2 in PIES. The same feature was observed previously for the n_{Br} bands of HBr,[27(b)] CH_2BrCl, and CH_2BrCN.[32]

The combination of SO interaction and Jahn-Teller effects[2] leads to a splitting of the outermost n_{Br} energy level of CH_3Br into two components ($e_{3/2}$ and $e_{1/2}$) separated by an energy interval of $\sim$0.33 eV. The related partial ionization cross sections exhibit the same negative collision energy dependence ($m=-0.34$) and indicate that the potential energy surface describing the interaction between the molecule and the He* probe is strongly attractive around the Br atom. Indeed, when the long-range attractive part of the interaction potential V^* is dominant and of the form

$$V^*(R) \propto R^{-s}, \tag{2}$$

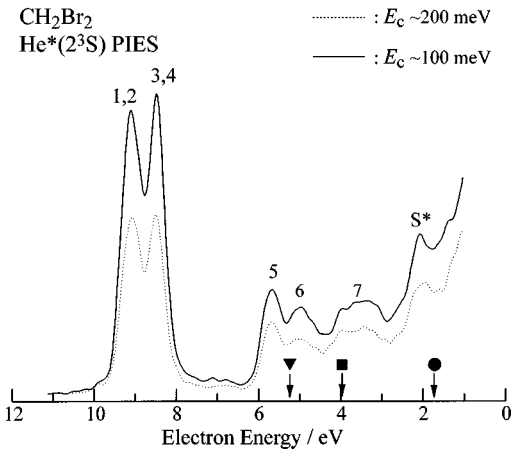

FIG. 5. Collision-energy-resolved He*($2\,^3S$) PIES of CH_2Br_2 (solid curve at 100 meV and dashed curve at 200 meV). Arrows indicate estimates of the energy of electrons released through autoionization of a Br* atom into the $^3P_2$ (▼), $^1D_2$ (■), and $^1S_0$ (●) states of the Br^+ ion (see text).

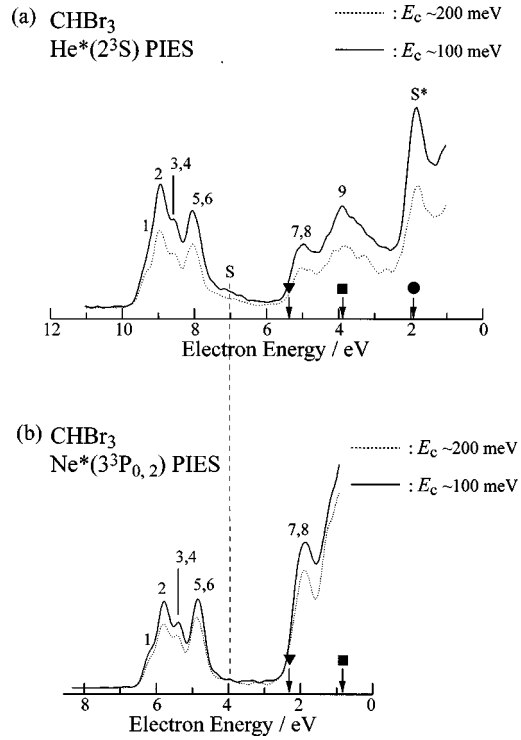

FIG. 6. Collision-energy-resolved PIES of $CHBr_3$ (solid curve at 100 meV and dashed curve at 200 meV) for (a) $He^*(2\,^3S)$ and (b) $Ne^*(^3P_{0,2})$. Arrows indicate estimates of the energy of electrons released through autoionization of a Br* atom into the $^3P_2$ (▼), $^1D_2$ (■), and $^1S_0$ (●) states of the Br^+ ion (see text).

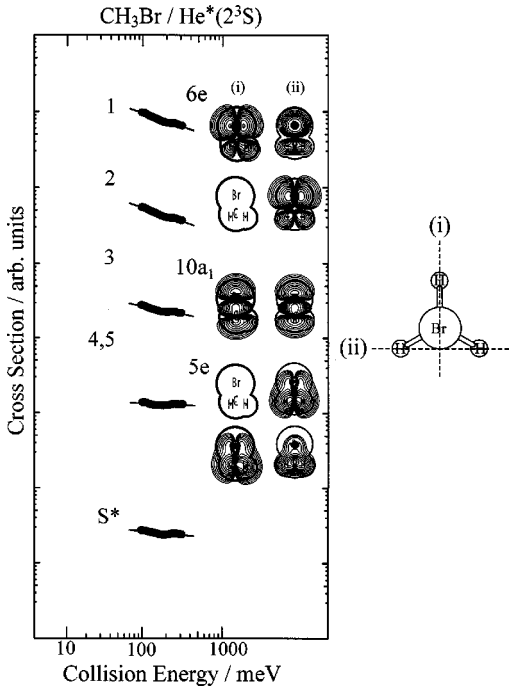

FIG. 7. Collision-energy dependence of the partial ionization cross sections for CH_3Br with $He^*(2\,^3S)$. Electron density maps are shown for respective MOs. Perpendicular cutting planes (i) and (ii) include H-C-Br bonds and two H atoms, respectively.

the collision-energy dependence of the partial ionization cross section $\sigma(E_c)$ can be expressed[7,11,16,17] as

$$\ln \sigma(E_c) \propto (-2/s) \ln E_c , \tag{3}$$

where $s=-2/m$ for atomic targets. The slope values obtained from CEDPICS measurements for ionization from the n_{Br} orbitals are similar for CH_3Br ($m=-0.34$), CH_2BrCl ($m=-0.35,-0.36$),[32] and CH_2BrCN ($m=-0.34$, -0.35)[32]—it thus appears that an analogy with atomic targets is justified, since the molecular environment has very limited influence. Correspondingly, an attractive potential well is observed in the model potential curve (Fig. 10) when the Li probe interacts with a Br atom, whatever the direction of the approach. Note that the well is the most strongly attractive when the probe approaches the bromine atom in a direction that is perpendicular to the C-Br bond. Compared with available UPS data, a peak shift (ΔE) of -150 meV for the n_{Br} bands confirms experimentally the existence of an attractive potential well of this order, in good agreement with the calculated well depths [Fig. 10(a)].

The third band in the PIES of CH_3Br can be assigned (Table I) to the $10a_1$ orbital on the basis of the OVGF and ADC(3) calculations. This orbital corresponds merely to the $\sigma_{C\text{-}Br}$ bond and exhibits therefore limited PIES intensity. In line with its more strongly localized nature and the EED results, this orbital is characterized by a reduced collision-energy dependence of the related partial ionization cross section ($m=-0.20$) compared with the lone-pair bands 1, 2. Since the slope of CEDPICS can be connected to the steepness of the potential curve ($s=-2/m$), a larger s value is correspondingly expected for band 3. Unsurprisingly therefore, the potential energy surface for the head-on access to the C-Br bond in the CH_3Br molecule is less attractive and shows a relatively smaller slope in the long-range region than the interaction potential for an approach along a perpendicular direction [Fig. 10(a)]. This result is consistent with the conclusions drawn previously in a similar study of the Penning ionization electron spectra of monohalogenobenzenes —C_6H_5X (X=F,Cl,Br,I)— (Ref. 22) upon collision with $He^*(2\,^3S)$ atoms. In this study, the most attractive interactions with incoming $He^*(2\,^3S)$ species were also found along axes that are perpendicular to the C-X bonds, with the exception of the C_6H_5F compound, for which the most energetically favorable direction approach is collinear with the C-F bond.

A very limited collision-energy dependence is observed (Table I) in CEDPICS ($m=-0.05$) and CERPIES measurements on the pair of ionization lines (4,5) arising from the doubly degenerate $5e$ (π_{CH_3}) level. Despite the limited resolution of the spectrometer, it is obvious from the band widths in the UPS and PIES records displayed in Fig. 1 that this doubly degenerate level is subject to very strong vibronic coupling effects. It is known that[15] the slope parameter m is related to the effective decay parameter d for the repulsive interaction potential [$V^*(R)=B\exp(-dR)$], where R represents the distance between the metastable atomic probe and a target molecule, and the effective parameter b for the transition probability [$W(R)=C\exp(-bR)$] through the relation

$$m=(b/d)-1/2. \tag{4}$$

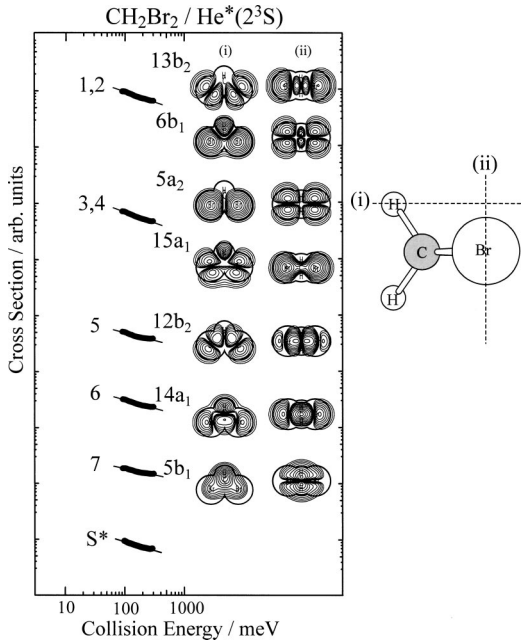

FIG. 8. Collision-energy dependence of partial ionization cross sections for CH_2Br_2 with He*($2\,^3S$). Electron density maps are shown for respective MOs. Perpendicular cutting planes (i) and (ii) include a H atom and two Br atoms, respectively.

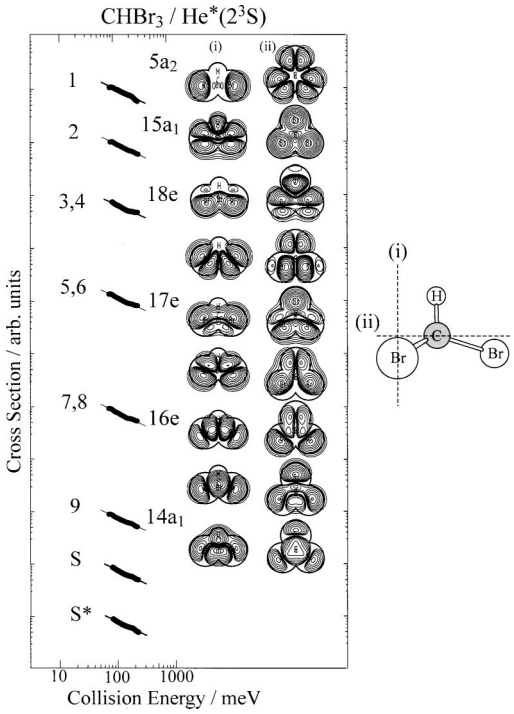

FIG. 9. Collision-energy dependence of partial ionization cross sections for $CHBr_3$ with He*($2\,^3S$). Electron density maps are shown for respective MOs. Perpendicular cutting planes (i) and (ii) include two Br atoms and the C atom, respectively.

Here, the effective parameter b derives from the first ionization potential[63,64] $[I(M)]$ via

$$b = 2\{2I(M)\}^{1/2}. \tag{5}$$

Therefore, the very limited slope of the CEDPICS characterizing bands 4, 5 indicates that the interaction potential that prevails around the π_{CH_3} MO region is mostly repulsive. This finding corroborates the model potential displayed in Fig. 10(a), which shows only a very shallow energy minimum at a relatively large $R_{\text{C-Li(He*)}}$ distance (5.0 Å), and foretells soft repulsive interactions when $R_{\text{C-Li(He*)}} < 4.0$ Å.

It is worth mentioning that in previous studies by counting of ion fragments produced in dissociative ionization processes of CH_3Cl and CH_3Br upon collision with Ne*($3\,^3P_{0,2}$) atoms,[65] the relatively limited collision-energy dependence of the CH_3^+, CH_2Cl^+, and CH_2Br^+ signals was already ascribed to a soft repulsive interaction around the methyl group. The results drawn here from a CEDPICS analysis and *ab initio* calculations confirm this assumption.

B. CH_2Br_2

The four outermost ionization bands (1–4) of CH_2Br_2 originate from n_{Br} lone-pair orbitals. Band 2 has larger PIES intensity than band 1, in very fair agreement with the EED spectrum (Fig. 2). All four n_{Br} bands (1–4) exhibit (Table II) CEDPICS slope parameters m and peak energy shifts ΔE similar to those reported in Sec. V A for the n_{Br} bands of CH_3Br ($m = -0.34$, $\Delta E = -150$ meV). On the other hand, the slightly stronger collision-energy dependence of the partial ionization cross sections of the $\sigma_{\text{C-Br}}$ bands (5 and 6) of CH_2Br_2 (Table II) reflects the overall more attractive nature of the interaction potential between CH_2Br_2 and He*($2\,^3S$), compared with the $\sigma_{\text{C-Br}}$ bands of CH_3Br (Table I). Indeed, with CH_2Br_2, an attractive interaction potential with a broader well is found in model potentials calculated along direction approaches that are perpendicular to the C-Br axis [see Fig. 10(b) versus Fig. 10(a)].

The ADC(3) calculations indicate a breakdown of the orbital picture of ionization for the nondegenerate $5b_1$ (π_{CH_2}) orbital of CH_2Br_2 ($m = -0.22$), in the form of a substantial dispersion of the ionization intensity into a shake-up line at ~16.4 eV. This breakdown corroborates a significant band broadening in the He I UPS on the experimental side (Fig. 2). A striking feature in the Penning ionization spectrum of CH_2Br_2, which is completely missing in the He I UPS and theoretical ADC(3) spectra, is a band (S*) at electron energies around 2 eV. As shall be shown in Sec. VI, this band relates to autoionization processes.

C. $CHBr_3$

Both with the OVGF and ADC(3) calculations for $CHBr_3$, the following ionization energy order was suggested for the six outermost levels of $CHBr_3$: $5a_2 < 18e < 15a_1 < 17e$. Because of spin-orbit (SO) interactions, the $18e$ orbital energies clearly appear in the UPS and PIES measurements (Fig. 3) as a pair of lines (bands 3, 4) separated by an energy interval of 0.38 eV, to compare with a well-known SO-splitting parameter of 0.305 eV for the bromine atom.[2] Thus band 2 can be ascribed to the $15a_1$ orbital ($n_{Br}\perp$, extending for the out-of-plane direction of the plane including three Br atoms). This fully symmetric orbital strongly protrudes outside the collision boundary surface (Fig. 9) and is characterized by a large EED value; unsurprisingly therefore,

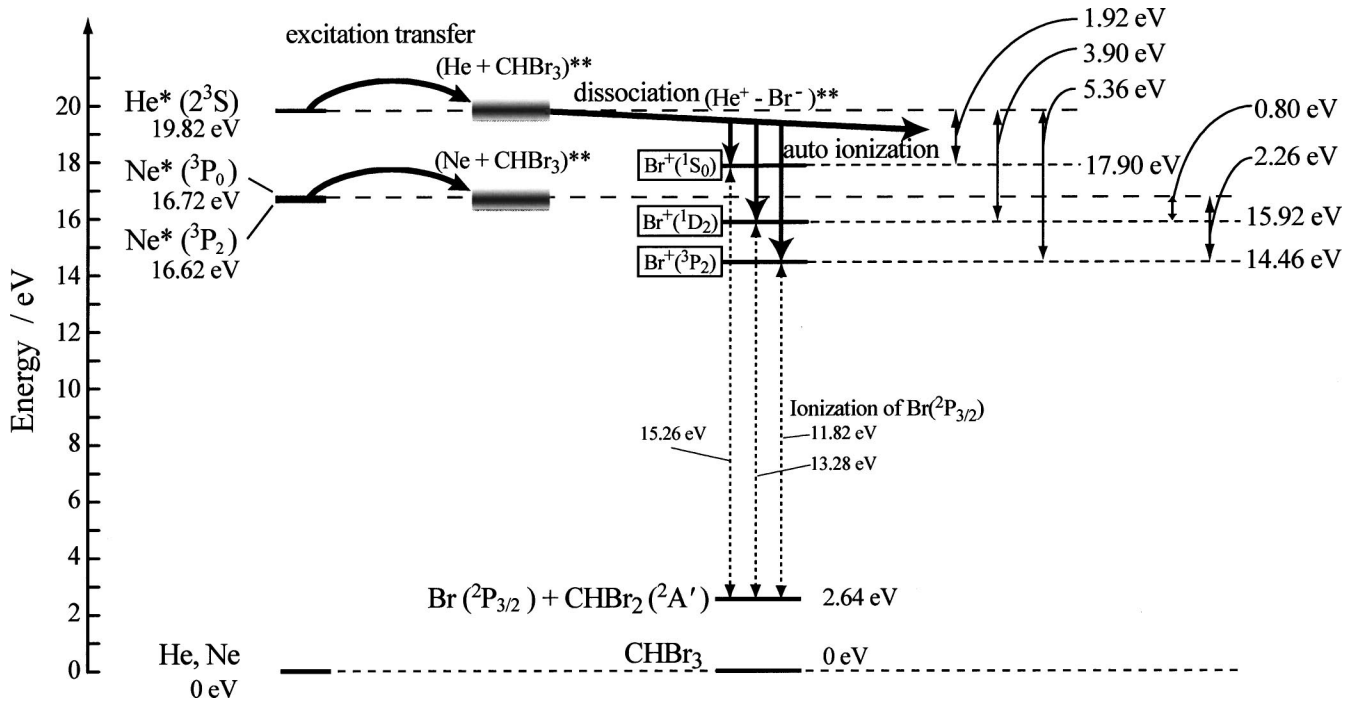

FIG. 11. Energy analysis of the dissociation and autoionization processes of $CHBr_3$ accounting for the S* bands in the He*($2\,^3S$) and Ne*($^3P_{0,2}$) PIES of Fig. 6.

band 2 has large PIES intensity (Fig. 3). On the other hand, band 1 in the PIES of $CHBr_3$ relates to an antisymmetric orbital ($5a_2$). Since the overlap with the He* 1*s* orbital vanishes at the nodal plane of the $5a_2$ MO, this band is characterized by a much more limited EED value and, thus, PIES intensity. All bands in the spectrum exhibit similar CEDPICS characteristics ($m \sim -0.48$), which reflects attractive and isotropic interactions around the molecule, in agreement with the calculated interaction potential curves [Fig. 10(c)]. In particular, it is noted that the interaction potential curve found for head-on access to the C-H bond of $CHBr_3$ is much more attractive than that calculated for the C-H bonds of CH_3Br [Fig. 10(a), see Sec. V A]. The larger PIES intensity of band 9 relative to that of bands 7, 8 (Fig. 3), in spite of the smaller EED value for the $14a_1$ orbital compared with that of the doubly degenerate 16*e* set, as well as a significant dispersion of the $14a_1$ ionization intensity over several shake-up lines with comparable spectroscopic strength, is due to overlapping autoionization S* bands (see Sec. VI). Note that, again, the breakdown of the molecular orbital picture which is predicted from the ADC(3) calculations for the $14a_1$ orbital of CH_3Br (Table III, Fig. 3) provides a consistent explanation to the large width of band 9 in He I UPS.

VI. ANALYSIS OF THE S* AND S AUTOIONIZATION BANDS

A broad extra band at an electron energy of ~2 eV has been observed previously [*B* band in Ref. 27(b)] in PIES measurements on HBr upon collision with He*($2\,^3S$) atoms, and has been ascribed to autoionization of an electron by the attractive potential of a transient ion pair (HBr^--He^+) into various ionic states. In particular, a sharp band structure in the PIES of HBr at an electron energy smaller than ~1.5 eV has been assigned to an excitation transfer to high-lying (Rydberg) states of HBr** Rydberg states dissociating into H(1*s*) and Rydberg Br** atoms which, in turn, decay through autoionization into Br^+ ($^1D_2$ or $^3P_{1,2}$) species.[27(b)] Very similarly, broad extra bands in the He*($2\,^3S$) PIES of HI have been assigned to ionic states of I^+ produced via autoionization within the potential energy surface of a transient HI^--He^+ ionic pair.[27(c)] S* bands with limited intensity have also been observed at electron energies smaller than ~2 eV in the He*($2\,^3S$) PIES of other halogenomethanes (CH_2BrCl and $CHBrCl_2$).[32] In the present study on bromomethanes, broad bands which very clearly do not correlate with one-electron or shake-up ionization states are seen at electron energies of ~1.0, ~2.1, and ~1.9 eV in the He*($2\,^3S$) PIES of CH_3Br, CH_2Br_2, and $CHBr_3$, respectively. The purpose of this section is to demonstrate that these S* bands relate to autoionization of Br* Rydberg atoms produced through dissociation of the molecular target.

In order to identify on clear grounds the various transitions involved in these processes, we compare in Fig. 11 the excitation energy level diagram of He and Ne with the ionization energy diagram of a bromine atom in its doublet electronic ground state ($^2P_{3/2}$), as established from He I UPS data,[66] and taking into account a theoretical estimate of 2.64 eV for the dissociation energy of $CHBr_3$ into Br($^2P_{3/2}$) and $CHBr_2$($^2A'$) radical species (this value has been obtained from single-point calculations at the benchmark CCSD(T) level [Ref. 67], in conjunction with the aug-cc-pVDZ basis set, on B3LYP/aug-cc-pVDZ geometries, and including a B3LYP/aug-cc-pVDZ correction of −0.112 eV for the change in zero-point vibrational energies). From this comparison, it is obvious that, regardless of vibrational complications, the electron energies released upon dissociation and

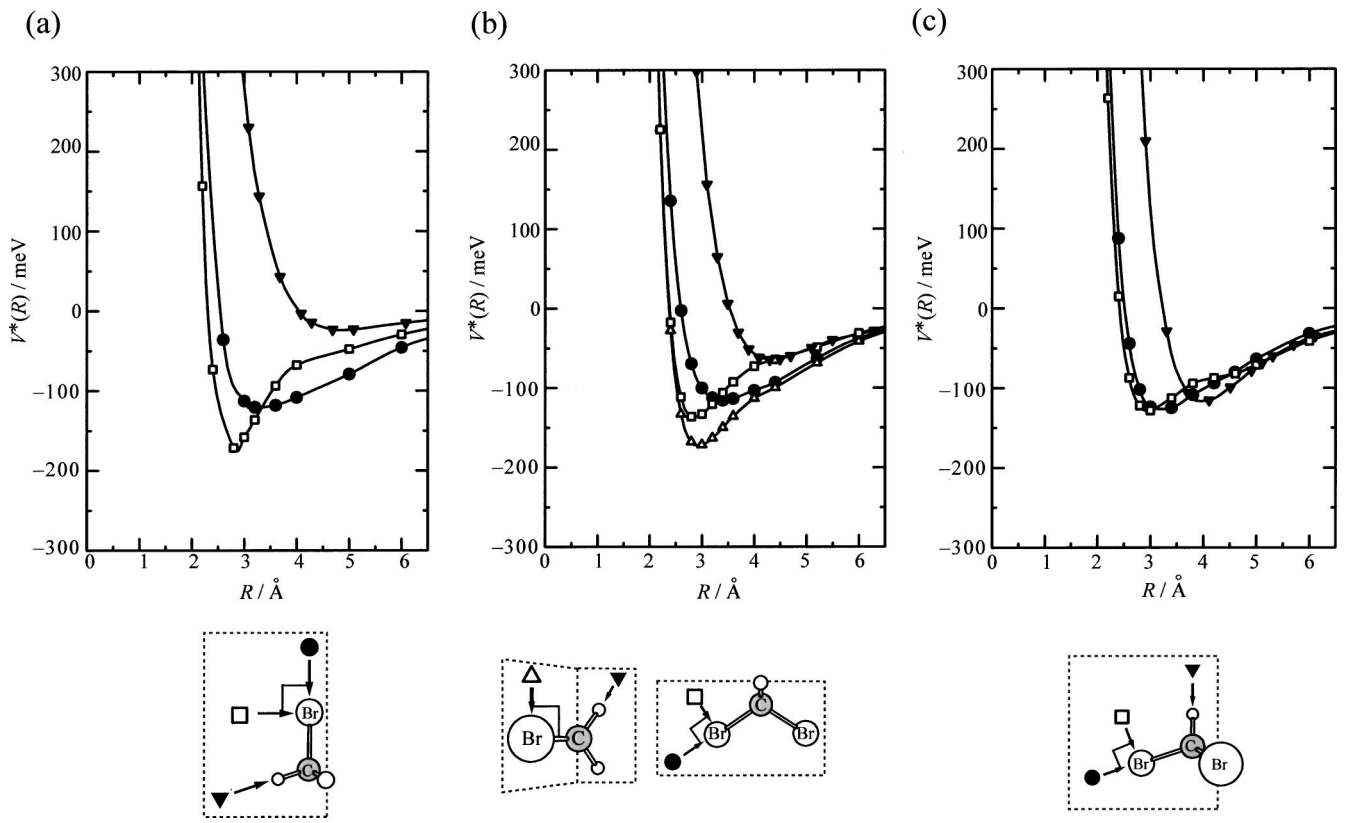

FIG. 10. Interaction potential curves $V^*(R)$ for the (a) CH_3Br-Li, (b) CH_2Br_2-Li, and (c) $CHBr_3$-Li systems, along various direction approaches. R is the distance between Li and Br or C atoms.

autoionization of a transient $(He^+\text{-}Br^-)^*$ ionic pair into He in its ground state ($^1S_0$) and the lowest electronic states of the Br^+ ion amount to 5.37 ($^3P_2$), 3.90 ($^1D_2$), and 1.92 eV ($^1S_0$). The S* band at an electron energy of ca. 1.9 eV in the He*($2\,^3S$) PIES of $CHBr_3$ (Fig. 3) can thus undoubtedly be assigned to the formation of a transient ionic pair ($Br^-\text{-}He^+$) and autoionization into the $Br^+(^1S_0)$-He state by the attractive potential of the He^+ ion. Also, autoionization into the $Br^+(^3P_2)$-He and $Br^+(^1D_2)$-He states provides a consistent explanation to the very large intensities of bands at electron energies of ~5 and ~3.7 eV, in contrast with the relatively limited intensities of bands 7, 8, and 9 in the simulation drawn from the exterior electron density model of electron exchange Penning ionization (see Fig. 3). When Ne*($3\,^3P_{0,2}$) metastable atoms are used for ionizing $CHBr_3$, autoionization energies of 2.26 ($^3P_2$) and 0.85 eV ($^1D_2$) are found (Fig. 11), which is consistent with the large electron counts at electron energies lower than ~2.0 eV in the Ne*($3\,^3P_{0,2}$) CERPIES of Fig. 6(b).

Many of the observations drawn from the analysis of the S* autoionization bands of $CHBr_3$ also prevail for CH_2Br_2. The CCSD(T)/aug-cc-pVDZ dissociation energy (2.78 eV [Ref. 68]) of this molecule into Br and CH_2Br radical species is very similar to that required for the homolytic cleavage of a C-Br bond in $CHBr_3$. Unsurprisingly therefore, the energy location of the autoionization S* band remains practically unchanged (~2.1 eV). Exactly as for bands (7,8) and 9 in the He*($2\,^3S$) PIES of $CHBr_3$, the relatively much too large intensity of band 7 in the He*($2\,^3S$) PIES of CH_2Br_2 compared with the EED simulation (Fig. 3) can be attributed to overlapping bands due to the decay of a transient ($He^+\text{-}Br^-$) ionic pair into He and Br^+ in their singlet ground (^1S) and triplet excited ($^3P_2$) states, respectively.

The negative collision-energy dependence of the partial ionization cross sections associated to the S* band of $CHBr_3$ ($m=-0.48$) and CH_2Br_2 ($m=-0.30$) indicates an attractive interaction for the entrance channel. Assuming that the generation of the intermediate ionic pair ($Br^-\text{-}He^+$) occurs at large distances between the molecular target (M) and the He* probe, and that the interaction potential that prevails therefore is of the Coulomb type ($s=1$), one should normally find values around -2 for the slope parameters characterizing the CEDPICS measurements on the S* bands of these two molecules. In reality, the obtained parameters are much smaller in absolute value ($m=-0.30$ and $m=-0.48$, respectively) and very comparable (Tables II and III) to those found for the n_{Br} and $\sigma_{C\text{-}Br}$ bands produced by electron-exchange-type ionization. Thus, it can be concluded that the generation of the ($Br^-\text{-}He^+$) ionic pair occurs at short-range distances between the bromine atoms in the molecular target and the He* probe, and that the unoccupied MOs of CH_2Br_2 and $CHBr_3$ having relation with this charge and excitation transfer are σ^* orbitals that are merely localized around the C-Br bonds. Contour plots at the HF/6-31+G* level suggest that the lowest unoccupied molecular orbitals (LUMO) of CH_2Br_2 [$16a_1$, Fig. 12(b)] and, almost, $CHBr_3$ [$16a_1$, Fig. 12(c)] are likely candidates for such electron transfer processes, since they show a strong

localization around the central and positively charge carbon atom and one nodal plane across the C-Br bonds. At this stage, it must be noted that unoccupied orbitals obtained at the HF level using a finite basis set represent only approximations to continuum functions. For molecules characterized, as here, by unbound or weakly bound anion states (see further), the shape of these orbitals is subject to rather significant changes upon improvements of the basis set, in particular the inclusion of diffuse functions (see, e.g., Ref. 69). It is thus worth noting that the 6-31+G* basis set already includes such functions.

In line with the previous estimates for $CHBr_3$ and CH_2Br_2, single-point CCSD(T)/aug-cc-pVDZ calculations on B3LYP/aug-cc-pVDZ geometries lead to a value of 2.92 eV [Ref. 70] for the radical dissociation energy of a C-Br bond in CH_3Br. In spite of this, the autoionization S* band of CH_3Br was observed at an unexpectedly low electron energy of about 1 eV. At this stage, it is worth recalling that autoionization bands of superexcited (Rydberg) Br** atoms have been observed at electron energies lower than 1.5 eV in the He*($2\,^3S$) Penning ionization spectrum of HBr.[27(b)] The CEDPICS characterizing the S* band of CH_3Br ($m=-0.10$) is intermediate to that seen for the $\sigma_{C\text{-}Br}$ ($m=-0.20$) and π_{CH_3} bands ($m=-0.05$), which reflects repulsive interactions in the entrance channel and, relatively to $CHBr_3$ [Fig. 12(c)] and CH_2Br_2 [Fig. 12(n)], a larger delocalization of the LUMO ($11a_1$) of CH_3Br, also a σ^* orbital, over the methyl group [Fig. 12(a)]. Note also that the more diffuse nature of that orbital reflects both its higher position in the continuum and the lesser positive charge on the central carbon atom of CH_3Br, compared with CH_2Br_2 and, almost, $CHBr_3$. Since the He*($2\,^3S$) probe reacts here as a nucleophilic species, the excitation and charge transfers leading to autoionization processes must therefore be less selective and efficient than in the case of CH_2Br_2 and $CHBr_3$. Relatedly, Br^+ ions have been scarcely observed[65] in Penning ionization studies of CH_3Br upon collision with Ne*($3\,^3P_{0,2}$) species, which indicates that the excitation energy of Ne*($3\,^3P_{0,2}$) is not sufficient for enabling excitation transfers into dissociative states of CH_3Br. In simpler words, CH_3Br has a too limited electron affinity for ionizing a Ne*($3\,^3P_{0,2}$) species.

With regards to the intensity of the S* bands in the PIES of $CHBr_3$ compared with that of the n_{Br} bands and $\sigma_{C\text{-}Br}$ bands nearby, the autoionization processes clearly overwhelm the electron exchange Penning ionization processes in this molecule at electron energies below ~6 eV. This is not entirely surprising, since it is known from electron transmission spectroscopy and continuum multiple scattering $X\alpha$ calculations that the electron affinity of bromomethanes increases with the number of Br atoms.[71] $CHBr_3$ has an electron affinity of 0.45 eV and, thus, a stable ground anion state.[71] In contrast, the lowest anion states of CH_2Br_2 and CH_3Br lie at ~0.2 and ~2.1 eV above the vacuum level, respectively,[67] and are thus subject to decay. Therefore, in the competition for intensity with the electron exchange Penning ionization processes in the $\sigma_{C\text{-}Br}$ electron energy region, the branching ratio towards autoionizing states produced via an intermediate Br^--He^+ ionic pair should logically be much larger for $CHBr_3$ than that for CH_3Br or CH_2Br_2. Indeed, for $CHBr_3$, the observed ratio between the relative intensities of the $\sigma_{C\text{-}Br}$ (7,8) and n_{Br} (1–6) bands in the PIE spectrum ($I^{obs}_{\sigma/n}=I^{obs}_{\sigma}/I^{obs}_{n}=0.379$) strikingly differs from the ratio based on EED estimations of these relative intensities ($I^{EED}_{\sigma/n}=I^{EED}_{\sigma}/I^{EED}_{n}=0.152$). Thus, the EED simulation underestimates the relative intensity of the $\sigma_{C\text{-}Br}$ (7,8) band by a branching ratio of $I^{obs}_{\sigma/n}/I^{EED}_{\sigma/n}=2.493$. For comparison, the branching ratio towards autoionizing states estimated in a similar way for CH_2Br_2 and CH_3Br only amounts to 1.67 (=3.06/1.83) and 1.33 (=3.76/2.83) only. The increase of the importance of autoionization processes with the number of bromine atoms reflects thus very well both a stronger localization of the LUMO around C-Br bonds, and an increase of the electron affinity.

A rather intense band is observed at ~1 eV below the electron energy (~7.1 eV) characterizing band 5, 6 in the He* PIES of $CHBr_3$ [Fig. 6(a)]. This band is clearly very different from the Frank-Condon vibrational progression associated to bands 5, 6 in the He I UPS (Fig. 3) and is characterized by a large negative collision-energy dependence ($m=-0.48$) of its partial ionization cross section. As this band has no equivalent in the available photoelectron spectra (He I UPS and He II UPS, Ref. 60) and in the theoretical ADC(3) one-electron and shake-up ionization spectrum of $CHBr_3$ (Fig. 3), it must also be ascribed to autoionization processes. Similar bands, at electron energies ~1 eV below the deepest lone pairs, have also been observed in the PIES of HI [Ref. 27(c)] and HCl (Ref. 29) obtained upon collision with He*($2\,^3S$) species. These extra bands have been assigned to autoionization of superexcited states of a (He-HX)** complex into vibrationally excited states of the HX^+ molecular ion in its electronic ground state. A large negative collision-energy dependence was found for the partial ionization cross section of that extra band in the case of HCl ($m=-0.38$),[29] which reflects a strongly attractive interaction and indicates that the attack occurred at the level of the n_{Cl} lone pairs. Compared with an unperturbed HCl molecule, the stretching of the HCl bond from 1.247 Å in the unperturbed HCl molecule to 1.45 Å in the most stable form of a model H-Cl-Li complex is equivalent to exciting HCl into its vibrational level $v=2$. For bromomethanes, the large negative collision-energy dependence of the S bands can be ascribed to a distortion of the interaction potential for the entrance channel by an avoided crossing between the He*-M and He-M** potential energy surfaces at longer C-Br bond length than the one in the equilibrium state.

The S band is clearly missing in the Ne*($3\,^3P_{0,2}$) CERPIES [Fig. 6(b)] of $CHBr_3$. This difference can be ascribed to the lower excitation energy of the Ne*($3\,^3P_{0,2}$) species, compared to that of the He*($2\,^3S$) species. Thus, the energy of the excitation transfer state (He-M)** is thought to be higher than that of Ne*. A similar observation had been made previously[27(c)] for the Frank-Condon vibrational structure described as a S band in the He*($2\,^3S$) PIES of HI. This band was also missing in Ne*($3\,^3P_{0,2}$) PIES.[27(c)]

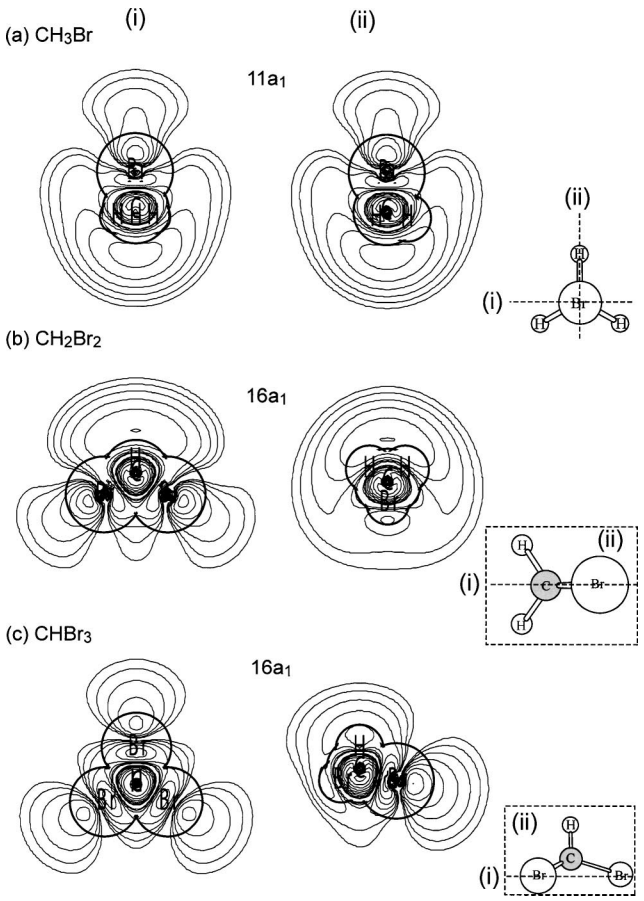

FIG. 12. The lowest unoccupied molecular orbital (LUMO) of (a) CH_3Br, (b) CH_2Br_2, and (c) $CHBr_3$.

VII. CONCLUSION

Bromomethanes (CH_3Br, CH_2Br_2, and $CHBr_2$) have been studied by means of collision-energy-resolved Penning ionization electron spectroscopy upon collision with metastable $He^*(2\,^3S)$ and, in the case of $CHBr_3$, $Ne^*(3\,^3P)$ atoms. The collision-energy dependence of partial ionization cross sections as well as model potential calculations indicate highly anisotropic interactions between He* and CH_2Br_2 or CH_3Br. For these molecules, the most energetically favorable trajectories for the He* probe are clearly along axes that intersect the C-Br bonds in a perpendicular way, at the level of the Br atom. On the other hand, near the collision boundaries, a soft repulsive interaction potential prevails around the methyl group of CH_3Br. In the case of $CHBr_3$, the interaction potential appears to be more isotropic.

A series of autoionization bands has been identified by comparison with He I UPS measurements and theoretical Green's Function calculations of one-electron and shake-up ionization spectra at the benchmark ADC(3)/aug-cc-pVDZ level. A first series of bands of the S* type has been observed in the $\sigma_{C\text{-}Br}$ region and at electron energies of ~1.9 and 2.1 eV in the $He^*(2\,^3S)$ Penning ionization electron spectrum of $CHBr_3$ and CH_2Br_2, respectively. These bands pertain to the dissociative decay of a transient ionic pair (Br^--He^+) into He in its ground state and an excited state of the Br^+ ion. For $CHBr_3$, and, to a lesser extent, for CH_2Br_2, autoionization processes lead to further bands that clearly overwhelm the $\sigma_{C\text{-}Br}$ or π_{CH_2} bands due to electron exchange Penning ionization processes. The collision-energy dependence of the relative intensity of the S* bands reflects the fact that an attractive interaction between the He* probe and the Br atoms of the target molecule prevails prior to the autoionization event. The S* band of CH_3Br is seen at an electron energy of ~1 eV, a value which is very similar to that found previously for the bands of HBr [Ref. 27(b)]. By analogy, this band has thus been ascribed to autoionization of superexcited Br** atoms into Br^+.

An autoionization band of the S type has also been identified in the He* PIES spectrum of $CHBr_3$, at ~1 eV below the deepest n_{Br} bands. By analogy with previous PIES studies of HI [Ref. 27(c)] and HCl,[29] this band has been assigned to the dissociation and autoionization of a superexcited $(He\text{-}Br\text{-}CHBr_2)^{**}$ complex into vibrationally excited states of the $CHBr_3^+$ molecular ion. Here also, the strongly negative collision-energy dependence of the related partial ionization cross section demonstrates that the interaction potential pertaining to the entrance channel in the autoionization process is also attractive.

ACKNOWLEDGMENTS

This work was supported by a Grant in Aid for Scientific Research from the Japanese Ministry of Education, Culture, Sports, Science and Technology. M.S.D. acknowledges support from the FWO_Vlaanderen, the Flemish branch of the National Science Foundation of Belgium.

[1] D. W. Turner, C. Baker, A. G. Baker, and C. R. Brundle, *Molecular Photoelectron Spectroscopy* (Wiley-Interscience, New York, 1970).
[2] J. H. D. Eland, *Photoelectron Spectroscopy: An introduction to Ultraviolet Photoelectron Spectroscopy in the Gas Phase* (Butterworth, London, 1974).
[3] J. W. Rabalais, *Principles of Ultraviolet Photoelectron Spectroscopy* (Wiley, New York, 1977).
[4] V. Čermák, J. Chem. Phys. **44**, 3781 (1966).
[5] A. J. Yencha, in *Electron Spectroscopy: Theory, Technique, and Applications*, edited by C. R. Brundle and A. D. Baker (Academic, New York, 1984), Vol. 5.
[6] H. Hotop and A. Niehaus, Z. Phys. **228**, 68 (1969).
[7] A. Niehaus, Adv. Chem. Phys. **45**, 399 (1981).
[8] K. Ohno, H. Mutoh, and Y. Harada, J. Am. Chem. Soc. **105**, 4555 (1983).
[9] K. Ohno, S. Matsumoto, and Y. Harada, J. Chem. Phys. **81**, 4447 (1984).
[10] K. Ohno and Y. Harada, in *Theoretical Models of Chemical Bonding*, edited by Z. B. Maksić (Springer, Berlin, 1991), Vol. 3.
[11] K. Mitsuke, T. Takami, and K. Ohno, J. Chem. Phys. **91**, 1618 (1989).
[12] K. Ohno, T. Takami, K. Mitsuke, and T. Ishida, J. Chem. Phys. **94**, 2675 (1991).
[13] A. Niehaus, Ber. Bunsenges. Phys. Chem. **77**, 632 (1973).
[14] K. Ohno, H. Yamakado, T. Ogawa, and T. Yamata, J. Chem. Phys. **105**, 7536 (1996).
[15] E. Illenberger and A. Niehaus, Z. Phys. B **20**, 33 (1975).
[16] M. R. Woodard, R. C. Sharp, M. Seely, and E. E. Muschlitz, Jr., J. Chem. Phys. **69**, 2978 (1978).
[17] T. Parr, D. M. Parr, and R. M. Martin, J. Chem. Phys. **76**, 316 (1982).
[18] L. Appolloni, B. Brunetti, J. Hermanussen, F. Vecchiocattivi, and G. G. Volpi, J. Chem. Phys. **87**, 3804 (1987).
[19] T. Takami, K. Mitsuke, and K. Ohno, J. Chem. Phys. **94**, 2675 (1991).
[20] K. Ohno, N. Kishimoto, and H. Yamakado, J. Phys. Chem. **99**, 9687 (1995).
[21] N. Kishimoto, K. Ohshimo, and K. Ohno, J. Electron Spectrosc. Relat. Phenom. **104**, 145 (1999).

[22] K. Imura, N. Kishimoto, and K. Ohno, J. Phys. Chem. A **105**, 4189 (2001).
[23] K. Imura, N. Kishimoto, and K. Ohno, J. Phys. Chem. A **105**, 6878 (2001).
[24] W. H. Miller and H. Morgner, J. Chem. Phys. **67**, 4923 (1977).
[25] W. Kischlat and H. Morgner, Z. Phys. A **312**, 305 (1983).
[26] K. Beckmann, O. Leisin, and H. Morgner, Mol. Phys. **59**, 829 (1986).
[27] (a) A. J. Yencha, J. Ganz, M. W. Ruf, and H. Hotop, Z. Phys. D: At., Mol. Clusters **14**, 57 (1989); (b) A. J. Yencha, M. W. Ruf, and H. Hotop, *ibid.* **21**, 113 (1991); (c) A. J. Yencha, M. W. Ruf, and H. Hotop, *ibid.* **29**, 163 (1994).
[28] B. Lescop, M. Ben Arfa, M. Cherid, G. Le Coz, G. Sinou, A. Le Nadan, and F. Tuffin, J. Phys. B **30**, 1241 (1997); B. Lescop, M. Ben Arfa, M. Cherid, G. Le Coz, G. Sinou, G. Fanjoux, A. Le Nadan, and F. Tuffin, J. Chem. Phys. **108**, 550 (1998).
[29] K. Imura, N. Kishimoto, and K. Ohno, J. Phys. Chem. A **106**, 3759 (2002).
[30] S. X. Tian, N. Kishimoto, and K. Ohno, J. Phys. Chem. A **107**, 485 (2003).
[31] S. X. Tian, N. Kishimoto, and K. Ohno, Chem. Phys. Lett. **365**, 40 (2002).
[32] S. X. Tian, N. Kishimoto, and K. Ohno, J. Phys. Chem. A **107**, 2137 (2003).
[33] N. Kishimoto, T. Horio, S. Maeda, and K. Ohno, Chem. Phys. Lett. **379**, 332 (2003).
[34] J. L. Gardner and J. A. R. Samson, J. Electron Spectrosc. Relat. Phenom. **8**, 469 (1976).
[35] K. Kimura, S. Katsumata, Y. Achiba, T. Yamazaki, and S. Iwata, *Handbook of He I Photoelectron Spectra of Fundamental Organic Molecules* (Japan Scientific, Tokyo, 1981).
[36] D. S. C. Yee, W. B. Stewart, C. A. Mcdowell, and C. E. Brion, J. Electron Spectrosc. Relat. Phenom. **7**, 93 (1975).
[37] H. Hotop and G. Hübler, J. Electron Spectrosc. Relat. Phenom. **11**, 101 (1977).
[38] N. Kishimoto, J. Aizawa, H. Yamakado, and K. Ohno, J. Phys. Chem. A **101**, 5038 (1997).
[39] G. Graner, J. Mol. Spectrosc. **90**, 216 (1975).
[40] D. Chadwick and D. J. Millem, J. Mol. Struct. **25**, 216 (1975).
[41] K. Tamagawa and M. Kimura, Bull. Chem. Soc. Jpn. **52**, 2747 (1979).
[42] L. Pauling, *The Nature of the Chemical Bond* (Cornell University, Ithaca, New York, 1960).
[43] (a) J. Schirmer, L. S. Cederbaum, and O. Walter, Phys. Rev. A **28**, 1237 (1983); (b) W. von Niessen, J. Schirmer, and L. S. Cederbaum, Comput. Phys. Rep. **1**, 57 (1984); (c) J. Schirmer and G. Angonoa, J. Chem. Phys. **91**, 1754 (1989); (d) H. G. Weikert, H.-D. Meyer, L. S. Cederbaum, and F. Tarantelli, *ibid.* **104**, 7122 (1996).
[44] M. W. Schmidt, K. K. Baldridge, J. H. Jensen, S. Koseki, M. S. Gordon, K. A. Nguyen, T. L. Windus, and S. T. Elbert, QCPE, Bull. **10**, 52 (1990).
[45] Duning's correlation consistent polarized valence basis set of double zeta quality (cc-pVDZ), augmented by a set of diffuse $\{s,p\}$ functions on hydrogens, a set of diffuse $\{s,p,d\}$ functions on carbons, and a set of diffuse $\{s,p,d\}$ functions on bromine atoms. The cc-pVDZ basis consists of a $[2s,1p]$ contraction of a $(4s,1p)$ primitive set on hydrogens, of a $[3s,2p,1d]$ contraction of a $(9s,4p,1d)$ primitive set on carbons, and of a $[5s,4p,2d]$ contraction of a $(14s,11p,6d)$ primitive set on bromines; see T. H. Dunning, Jr., J. Chem. Phys. **90**, 1007 (1989); R. A. Kendall, T. H. Dunning, Jr., and R. J. Harrison, *ibid.* **96**, 6796 (1992); A. K. Wilson, D. E. Woon, K. A. Peterson, and T. H. Dunning, Jr., *ibid.* **110**, 7667 (1999).
[46] M. S. Deleuze, Int. J. Quantum Chem. **93**, 191 (2003).
[47] B. Liu, Lawrence Berkely Laboratory Report No. LBL-8158 (unpublished); F. Tarantelli, A. Sgamellotti, L. S. Cederbaum, and J. Schirmer, J. Chem. Phys. **86**, 2201 (1987).
[48] L. S. Cederbaum and W. Domcke, Adv. Chem. Phys. **36**, 205 (1977); W. von Niessen, J. Schirmer, and L. S. Cederbaum, Comput. Phys. Rep. **1**, 57 (1984); J. V. Ortiz, J. Chem. Phys. **89**, 6348 (1988); V. G. Zakrzewski and W. von Niessen, J. Comput. Chem. **14**, 13 (1993).
[49] M. J. Frisch, G. W. Trucks, H. B. Schlegel *et al.*, GAUSSIAN98 (Revision A.7) (Inc., Pittsburgh, PA, 1998).
[50] A. D. Becke, J. Chem. Phys. **98**, 5648 (1993); C. Lee, W. Yang, and R. G. Parr, Phys. Rev. B **37**, 785 (1988).
[51] See, e.g., J. M. L. Martin, J. El-Yazal, and J.-P. François, Mol. Phys. **86**, 1437 (1995); M. G. Giuffreda, M. S. Deleuze, and J.-P. François, J. Phys. Chem. A **103**, 5137 (1999).
[52] E. W. Rothe, R. H. Neynaber, and S. M. Trujillo, J. Chem. Phys. **42**, 3310 (1965).
[53] H. Hotop, Radiat. Res. **59**, 379 (1974).
[54] H. Haberland, Y. T. Lee, and P. E. Siska, Adv. Chem. Phys. **45**, 487 (1981).
[55] H. Hotop, T. E. Roth, M.-W. Ruf, and A. J. Yencha, Theor. Chem. Acc. **100**, 36 (1998).
[56] A. W. Potts, H. J. Lempka, D. G. Streets, and W. C. Price, Philos. Trans. R. Soc. London, Ser. A **268**, 59 (1970).
[57] J. L. Ragle, I. A. Stenhouse, D. C. Frost, and C. A. Mc-Dowell, J. Chem. Phys. **53**, 178 (1970).
[58] R. N. Dixon, J. N. Murrell, and B. Narayan, Mol. Phys. **20**, 611 (1971).
[59] R. Manne, K. Wittel, and B. S. Mohanty, Mol. Phys. **29**, 485 (1975).
[60] W. von Niessen, L. Asbrink, and G. Bieri, J. Electron Spectrosc. Relat. Phenom. **26**, 173 (1982).
[61] C. E. Brion, W. B. Stewart, D. S. C. Yee, and P. Crowley, J. Electron Spectrosc. Relat. Phenom. **23**, 399 (1981).
[62] T. N. Olney, W. F. Chan, G. Cooper, C. E. Brion, and K. H. Tan, J. Electron Spectrosc. Relat. Phenom. **66**, 83 (1993).
[63] N. C. Handy, M. T. Marron, and H. J. Silverstone, Phys. Rev. **180**, 45 (1969).
[64] M. M. Morrell, R. G. Parr, and M. Levy, J. Chem. Phys. **62**, 549 (1975).
[65] B. Brunetti, P. Candori, J. De Andres, F. Pirani, M. Rosi, S. Falcinelli, and F. Vecchiocattivi, J. Phys. Chem. A **101**, 7505 (1997).
[66] K. Kimura, T. Yamazaki, and Y. Achiba, Chem. Phys. Lett. **58**, 104 (1978).
[67] Coupled cluster theory with single and double excitations and a perturbative estimate of triple excitations; see G. D. Purvis and R. J. Bartlett, J. Chem. Phys. **76**, 1910 (1982); G. E. Scuseria, C. L. Janssen, and H. F. Schaefer III, *ibid.* **89**, 7382 (1988); K. Raghavachari, G. W. Trucks, M. Head-Gordon, and J. A. Pople, Chem. Phys. Lett. **157**, 479 (1989); R. J. Bartlett, J. Phys. Chem. **93**, 1697 (1989).
[68] Value obtained from single-point calculations on B3LYP/aug-cc-pVDZ geometries, and including a B3LYP/aug-cc-pVDZ correction of -0.154 eV for the change in zero-point vibrational energies.
[69] M. S. Deleuze, M. G. Giuffreda, J.-P. François, and L. S. Cederbaum, J. Phys. Chem. A **104**, 1588 (2000).
[70] Including a B3LYP/aug-cc-pVDZ correction of -0.193 eV for the change in zero-point vibrational energies.
[71] A. Modelli, F. Scagnolari, G. Distefano, D. Jones, and M. Guerra, J. Chem. Phys. **96**, 2061 (1992).